

Lattice strain in oxidized Si nanostructure arrays from X-ray measurements

S. Tanaka^a, C.C. Umbach^a, Q. Shen^b, J.M. Blakely^{a,*}

^a*Materials Science and Engineering, Cornell University, Ithaca, NY 14853, USA*

^b*Cornell High Energy Synchrotron Source (CHESS), Cornell University, Ithaca, NY 14853, USA*

Abstract

Although lattice strains in oxidized wafers can be detected by optical and X-ray methods the measurement of strains in non-planar structures such as occur in Si devices is more difficult. We describe a novel technique for measuring such strains and report results for oxidized Si. In our work we have fabricated regular arrays of Si pillars on a Si(001) surface and measured the strain in the individual pillars induced by oxidation. The pillars have diameters of the order 100 nm and spacing of ~ 300 nm. With high resolution X-ray techniques this spacing is sufficiently small to allow the 'superlattice' diffracted beams from the fabricated structure to be well resolved. We measure the strain from the displacement of this superlattice diffraction pattern relative to the normal allowed bulk reflections. We report results for different combinations of Si pillar diameter and oxide thickness. Differential thermal contraction also contributes to the strain. The measured strains are of the order of 10^{-4} . Our results are in good agreement with simulations based on current models of Si oxidation. © 1999 Elsevier Science S.A. All rights reserved.

Keywords: Silicon; Silicon oxide; Stress; X-ray diffraction

1. Introduction

Thermal oxidation plays a key role in Si-based device technology [1–3]. In this paper we focus on the elastic strains induced in a three-dimensional Si structure due to oxidation at high temperatures and subsequent cooling. The strain results from two effects, viz. (i) the approximately 120% increase in volume per Si accompanying the formation of SiO_2 , and (ii) the decrease, by a factor of ~ 5 , in the thermal expansion coefficient upon oxidation. The strain in planar Si wafers, due to oxidation, can be monitored from wafer bending as detected by optical beam deflection [4,5]. However in real device structures, the Si–oxide interface is not always planar and other techniques are needed to study strains associated with such features, particularly at the nanoscale level. The experiments that we describe here use X-ray diffraction to detect lattice strain. Our method differs from conventional X-ray measurements of lattice parameter shifts, in that we study the diffraction from a two-dimensional regular array (or grating) of nominally identical surface features and measure how the entire

diffraction pattern from this array is affected by oxidation and cooling.

The difference expected in the oxidation-induced strain between planar and non-planar structures should be emphasized. Thermal oxidation of flat Si wafers at temperatures where the oxide has relatively large viscosity results in a compressive stress in the oxide and corresponding tensile stress in the Si. Cooling the wafer to room temperature causes the Si to contract more than the oxide coating and hence a further increase in the Si tensile stress. In the case of a Si cylinder or truncated cone (the approximate shape used in our experiments) the compressive stress in the oxide at the interface during oxidation causes the Si to be under compression, in the radial direction, rather than tension; the cooling step decreases the magnitude of the compressive stress and may even reverse the sign. Fig. 1a is a schematic of a truncated cone with an oxide coating while Fig. 1b is an SEM micrograph of the arrays used in our experiment.

2. Materials and methods

Within the standard kinematical theory of diffraction [6], the X-ray intensity scattered from a two-dimensional grating of Si pillars with spacings L_x and L_y and with $N \times N$

* Corresponding author. Tel.: + 1-607-255-5149; fax: + 1-607-255-2365.

E-mail address: blakely@msc.cornell.edu (J.M. Blakely).

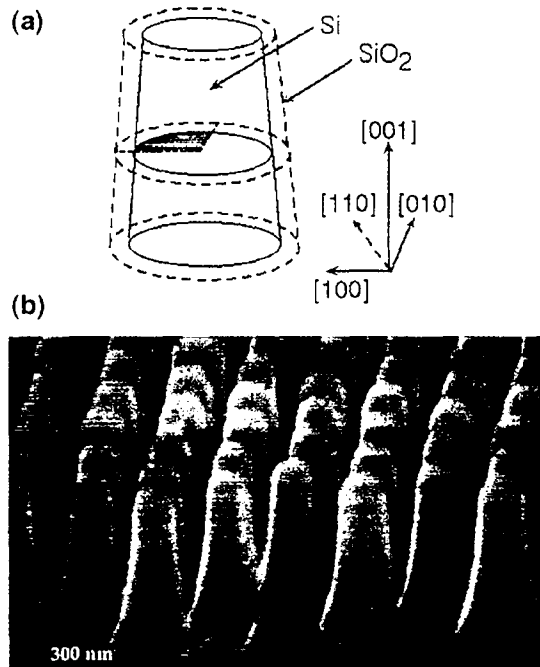


Fig. 1. (a) Approximate shape of the individual repeating units of the two-dimensional gratings used in these experiments. The formation of a surface oxide at low temperature causes both the oxide and the Si to be under compression in the radial direction. (b) Scanning electron micrograph of a grating of pillars of 400 nm spacing used in the experiment.

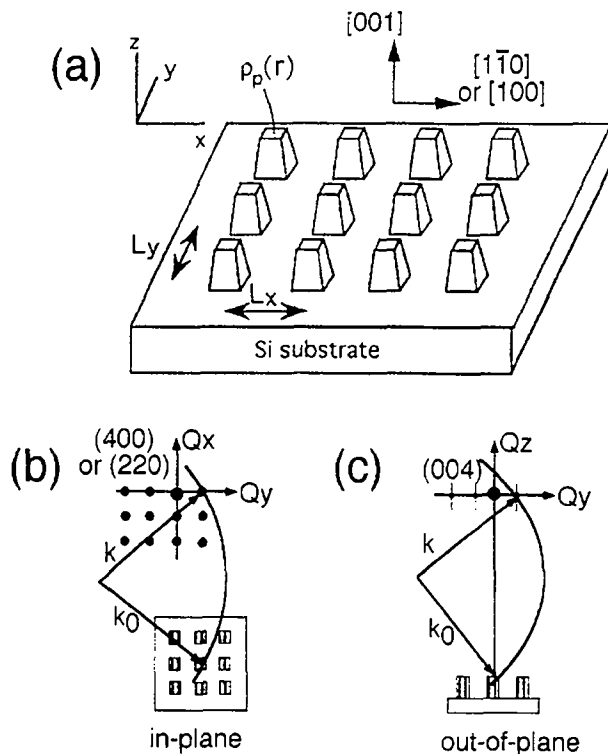


Fig. 2. (a) Schematic of a two-dimensional grating on a Si(001) surface; (b,c) indicate the geometry of the X-ray diffraction experiment. k_0 and k represent the incident and scattered wave vectors; (b) shows the glancing incidence case while (c) shows the symmetrical reflection case.

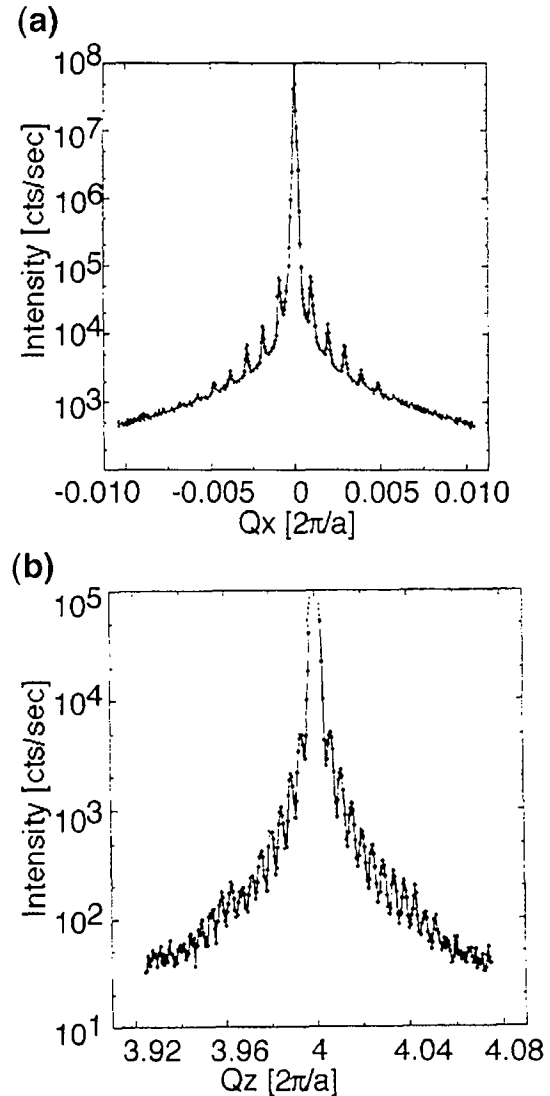


Fig. 3. Line scans of the intensity variation from an unoxidized Si grating near the Si(004) reflection; (a) is taken along [110] (parallel to the surface), while (b) is taken along [001] (normal to the surface).

pillars coherently illuminated, is given by [7]

$$I(Q) = |f(Q)|^2 \left\{ \frac{\sin(NQ_x L_x/2)}{\sin(Q_x L_x/2)} \right\}^2 \times \left\{ \frac{\sin(NQ_z L_z/2)}{\sin(Q_z L_z/2)} \right\}^2 \quad (1)$$

$f(Q)$ is the scattering form factor for a single pillar. Q is the scattering wave vector with orthogonal components Q_x and Q_z parallel to the mean surface. The scattering form factor for the individual pillars is peaked at the normal allowed Bragg reflections so that the intensity represented by the above equation is that of the crystal reflections and superimposed grating reflections. In a real diffraction experiment there will of course also be a contribution to the measured X-ray intensity from the underlying bulk crystal. With a grating of spacing ~ 300 nm the grating peaks are separated by angular amounts that are of the order of 10^{-3}

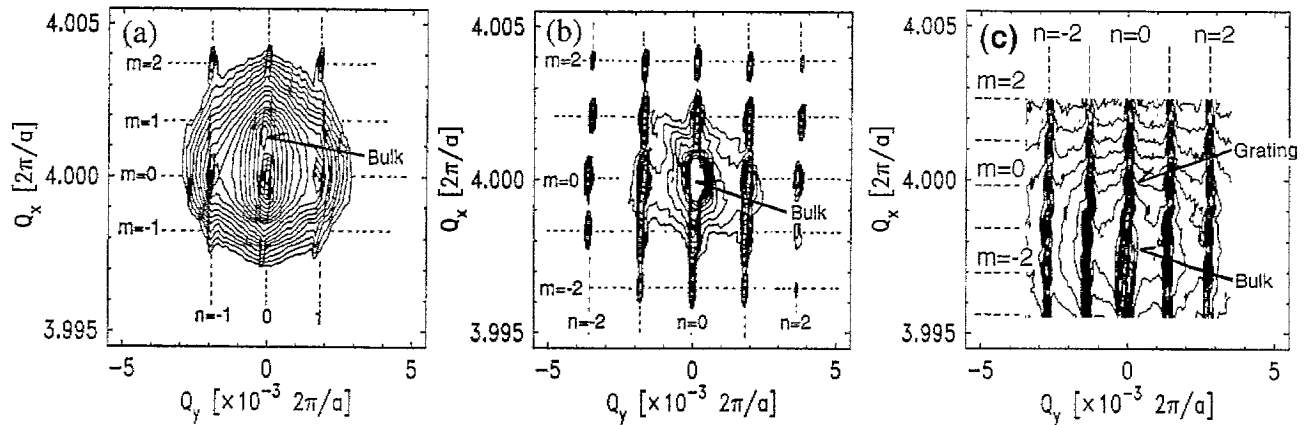


Fig. 4. Intensity distributions in a plane parallel to the sample (001) surface; (a) shows the intensity from a grating of 300 nm period, pillar radius 75 nm and oxide thickness 5 nm. Note the displacement of the 'center' of the grating pattern from the Si(004) reflection due to the elastic strain in the pillars; the direction of the displacement indicates a tensile strain in the Si. In (b) with the oxide removed by an HF dip the strain is relaxed; (c) shows the effect of a thicker oxide. Here the pillar spacing is ~ 400 nm, radius 100 nm and oxide thickness 15 nm; the offset of the bulk reflection and center of the grating pattern indicates a compressive strain.

times smaller than the lattice Bragg reflections. Fig. 2 shows the experimental scattering geometry and Fig. 3a is the measured intensity variation from a grating of unoxidized pillars near the (004) reciprocal lattice point scanning along [110] (the Q_x direction) using a monochromated synchrotron beam as described in Ref. [7]. Fig. 3b is an intensity measurement when scanning along the direction of the surface normal, Q_z , at $Q_x = 0$. Fig. 4 shows measured two-dimensional intensity contours near the reciprocal lattice point (Q_x, Q_y) = (4, 0) in a plane parallel to the mean surface for two different sample conditions. Fig. 4a corresponds to a grating of spacing 300 nm, Si pillar radius of ~ 75 nm and oxide thickness of ~ 5 nm; Fig. 4b is taken after removing the oxide with an HF dip. The oxidation was carried out at 850°C in dry O_2 and the oxide thickness was taken to be the same as that on planar regions of the sample. It should be noted that the 'center' of the diffraction pattern for the grating of strained pillars is displaced from the bulk (400) reflection while they coincide with the oxide removed. The average radial strain in the pillars is thus measurable from this measured displacement. (The axial strain can also be obtained from intensity scans of the type shown in Fig. 3b along the direction of the surface normal; only a limited amount of this type of data has been obtained). Fig. 4c shows a corresponding plot for a grating of pillars of spacing 400 nm in which the Si radius is ~ 100 nm and the oxide thickness ~ 15 nm; note that in this case the displacement of the grating pattern is opposite to that in Fig. 4a.

3. Results and discussion

The displacement of the grating diffraction pattern from the normal bulk reflections constitutes the experimental demonstration of the presence of stress in oxidized pillar arrays. The directions of the displacements, measured at

room temperature, for the different combinations of pillar radius and oxide thickness are interpreted to correspond to a tensile strain of $\sim 3.7 \times 10^{-4}$ in the Si core of the 75 nm radius pillars with 5 nm of oxide and a corresponding compressive strain of $\sim 4 \times 10^{-4}$ in the 100 nm pillars with 15 nm of oxide. These values can be understood in terms of currently accepted models of Si oxidation and known values of the thermal expansion coefficients [1].

3.1. Stress generated during oxidation

During oxide growth a radial compressive stress develops in the Si pillars due to the greater molar volume of the oxide coating. Based on previous studies with flat wafers [4,5] viscous flow in the oxide is sufficiently slow below $\sim 960^\circ\text{C}$ that the stress is not fully relaxed during oxidation. At the temperature of our oxidation process, 850°C, the viscosity of $\sim 1.3 \times 10^{16}$ poise (1 poise = 0.1 Pa s) [8] is such that little stress relaxation occurs. The development of stress during the oxidation process was computed using the semiconductor device simulation program TSUPREM-4 developed by Technological Modeling Associates. The program is based on the Deal-Grove model and includes the effect of surface orientation on the oxide growth rate [1]. The diffusivity of the oxidant in the oxide and the viscosity of the oxide are adjusted during growth to reflect the dependence of these parameters on stress. Fig. 5 shows the results of finite element computations for the stress distribution in Si cylinders corresponding to the experimental data of Fig. 4; since the cylinder axes are along [100] the computations can take advantage of the 4-fold rotation symmetry. Fig. 5a shows the stress distribution for a cylinder radius of 75 nm and oxide thickness 5 nm (achieved after 8 min at 850°C) while Fig. 5b corresponds to a radius of 100 nm and oxide thickness 15 nm (achieved after 45 min at 850°C). Due to the faster oxide growth rate in the [011] direction the

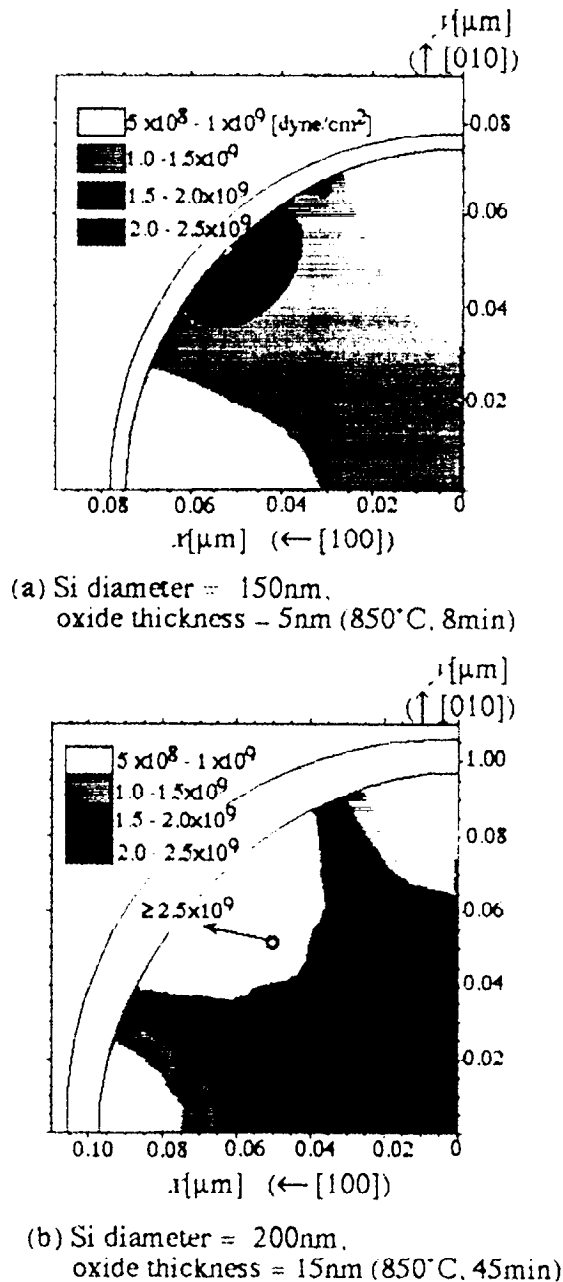


Fig. 5. Computed stress distributions (using TSUPREM-4) in a Si cylinder at the growth temperature on which an oxide layer has been grown at 850°C. $10 \text{ dyne/cm}^2 = 1 \text{ N/m}^2$. In (a) the oxide thickness is 5 nm while in (b) it is 15 nm. Due to the 4-fold symmetry about the [001] axis only one quadrant is shown. The maximum in the stress at the Si-SiO₂ interface is due to the greater oxide thickness on the (110) surface of the cylinder.

computed stress is non-uniform; in Fig. 5a the average stress is near $1 \times 10^9 \text{ dyne/cm}^2$ ($= 10^8 \text{ N/m}^2$) while in Fig. 5b the average is $\sim 2 \times 10^9 \text{ dyne/cm}^2$.

3.2. Stress due to differential thermal contraction

Since the thermal expansion coefficients of Si and of SiO₂ differ by a factor of ~ 5 (Si: $2.6 \times 10^{-6}/^\circ\text{C}$, SiO₂: $0.52 \times 10^{-6}/^\circ\text{C}$), in cooling from the oxidation temperature

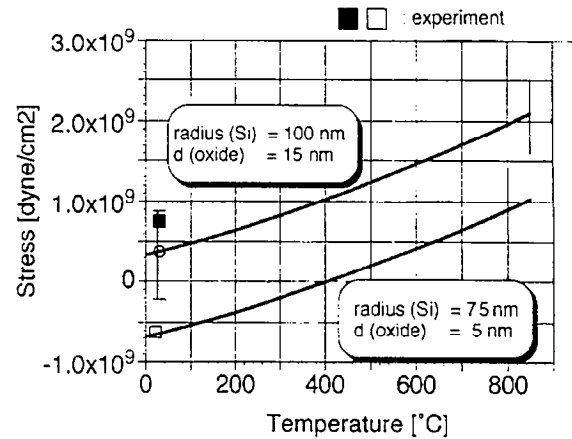


Fig. 6. Effect of differential thermal contraction on the stress in an oxide coated Si cylinder, for the parameters corresponding to Fig. 5, when the cylinder is cooled to room temperature. The greater percentage contraction of the Si causes the sign of the stress to be reversed on cooling while with the thicker oxide the initial compression is large enough that the stress remains compressive at room temperature. This trend is in agreement with the experiment as seen by comparing with the data of Fig. 4.

of 850°C to room temperature, the Si tends to contract by a larger percentage than the oxide. This effect alone would cause a tensile stress in the Si. The change in the stress of the inner cylinder can be computed using an analytical model developed by Warwick [9]. In using this model we have ignored the orientation dependence of the oxide thickness which is not a major effect. Fig. 6 shows the stresses predicted as a function of temperature for the two cylinders corresponding to Fig. 4a,c; the room temperature experimental data points are also shown. The agreement between the experiment and the computed stresses is reasonable in light of the number of parameters that are required in the simulation of the oxidation process. It is noteworthy that a compressive stress is predicted and observed for the thicker oxide coating, while the sign of the stress for the thinner oxide coating is reversed on cooling, also in agreement with the experiment.

In carrying out the stress calculations we have assumed the pillars to be cylindrical and to have a height much greater than the radius so that end effects are negligible. As seen in Fig. 2b the height to radius ratio was actually ~ 6 and the oxide also grew on the top surface of each pillar. While these discrepancies certainly affect the details of both the experimentally measured strains and computed stresses, the correspondence between experiment and model predictions lends support to the Deal-Grove oxidation model. Further work in which the stress is measured over a range of oxide thicknesses and at different oxidation temperatures would certainly be desirable.

Although we believe this work to be the first quantitative measurement of a compressive strain induced in Si nanostructures by oxidation, it has been recognized for some time that such strains exist. The work of Marcus et al. [3] and others [10] on the formation of sharp Si emitter-type tips

relies on the effect of large compressive stresses in Si cylinders to retard oxidation rates as the cylinder radius becomes extremely small.

The application of our method to measure the strains induced by oxidation in other materials, such as Ge–Si alloys, would certainly be of interest in giving clues to the mechanism of oxidation.

4. Summary and conclusions

We have described a novel method for making strain measurements in non-planar configurations. The method is based on making a 1- or 2D periodic array of the features under study and then measuring the displacement of the array X-ray reflections as oxidation takes place. Future work could involve arrays of trench structures and diffraction data collected during oxidation. The results demonstrate that compressive stresses are induced in the Si by oxidation. The magnitudes depend on oxide thickness and are in at least qualitative agreement with predictions from SUPREM, a commonly used oxide growth simulation program. The combination of oxidation induced stress and stress due to differential thermal contraction results in a room temperature stress that is very dependent on geometry and oxide thickness.

Acknowledgements

This work was supported by NSF grant DMR-9725082 and by the Cornell Center for Materials Research. The facilities of the CHESS and the Cornell Center for Nanofabrication, CNF, played key roles in the work. S.T. acknowledges support from Sumitomo Corp. We are grateful to Peter Griffin of Stanford University, and Mike Thompson, Matty Korhonen and Toshi Mogi of Cornell for help in stress simulations.

References

- [1] S.M. Sze, *VLSI Technology*, McGraw-Hill, New York, 1988.
- [2] D.-B. Kao, J.P. McVittie, W.D. Nix, K.C. Saraswat, *IEEE Trans. Electron Devices* ED-34 (1987) 1008.
- [3] R.B. Marcus, et al., *Appl. Phys. Lett.* 56 (1990) 236.
- [4] E.P. EerNisse, *Appl. Phys. Lett.* 30 (1977) 290.
- [5] E. Kobeta, E.A. Irene, *J. Vac. Sci. Technol. B* 6 (1988) 574.
- [6] B.E. Warren, *X-ray Diffraction*, Addison-Wesley, New York, 1969.
- [7] Q. Shen, C.C. Umbach, B. Weselak, J.M. Blakely, *Phys. Rev. B* 48 (1993) 17967.
- [8] A. Fargeix, G. Ghibaudo, *J. Appl. Phys.* 54 (1983) 7153.
- [9] C.M. Warwick, *J. Mater. Sci.* 26 (1991) 3817.
- [10] C.C. Umbach, B.W. Weselak, J.M. Blakely, Q. Shen, *J. Vac. Sci. Technol. B* 14 (1996) 3420.